



*Proceedings of the
Annual Stability Conference
Structural Stability Research Council
Charlotte, North Carolina, April 11-14, 2023*

Stability Considerations of Laser Fused Unequal-Leg Angle Stainless Steel Columns

Max E. Laracuenté¹, Edward J. Sippel², Hannah B. Blum³

Abstract

There is limited research on the stability behavior and design of stainless steel unequal leg angles in compression. As such, AISC 370: Specification for Structural Stainless Steel Buildings Chapter E is limited to equal-leg angle sections and requires the consideration of flexural-torsional stability in contrast to the previous Design Guide 27 recommendations from 2013. This paper reports on an experimental investigation on the stability considerations of laser-fused unequal-leg angle stainless steel columns to complement a related test series on hot-rolled unequal-leg angles. A series of unequal-leg angles with cross-sectional dimensions of 76.2 x 50.8 x 6.35 mm (3" x 2" x 1/4") and lengths ranging from 254 mm (10") to 3759 mm (148") were tested in compression. From these tests, the ultimate loads were recorded in addition to displacements, twists, and failure modes through the use of strain gauges and an optical tracking system. A series of tensile coupon tests were conducted to obtain the material properties, and the residual stress distributions were measured by the sectioning method. The results obtained from this investigation will serve to expand the limited research on the stability behavior of unequal-leg angles in compression.

1. Introduction

The recent release of American Institute of Steel Construction (AISC) Specification for Structural Stainless Steel Buildings (AISC, 2021) has provided additional opportunities to implement stainless steel members and take advantage of corrosion resistance, thermal properties, and aesthetics among other benefits (Houska, 2014). The Specification provides an updated design procedure to evaluate members in compression including compact, equal-leg single angles. Unlike carbon steel members designed according to AISC 360 (AISC, 2016), the stainless steel provisions incorporate a three stage buckling model that separates the response into full member yield, inelastic buckling, and elastic buckling. Another modification to the design procedure is the consideration of flexural-torsional buckling with single angles. The design provisions for carbon steel single angles permit excluding the direct calculation of flexural-torsional buckling, unless the legs are highly slender, since the local buckling reduction adequately reduces the flexural buckling capacity. Galambos

¹Former Graduate Research Assistant, University of Wisconsin-Madison

²Assistant Professor, Milwaukee School of Engineering, <sippel@msoe.edu>. Formerly, Graduate Research Assistant, University of Wisconsin-Madison

³Assistant Professor and Alain H. Peyrot Fellow, University of Wisconsin-Madison, <hannah.blum@wisc.edu>

(1991) demonstrated how this combination of flexural and local buckling results in the safe design of single angles. Previous design recommendations for stainless steel, provided in the 2013 edition of Design Guide 27 (Baddoo, 2013), were formulated following the carbon steel provisions and extended the same exception to stainless steel single angles. While some variations exist between the previous and current approaches, one consistent factor is that unequal-leg angles are beyond the scope of the design procedures due to limited relevant research.

In recent years, a growing amount of research on stainless steel equal-leg angles subjected to uniform compression has been completed. Early stub column tests of austenitic cold-formed angles by Kuwamura (2003) captured failure at greater than nominal yield stresses by flexural-torsional buckling for short columns. Sun et al. (2019) captured a similar response with hot-rolled stub column tests incorporating multiple grades. Various researchers have completed experiments capturing flexural-torsional buckling at shorter spans and flexural buckling for longer lengths including duplex laser-welded angles (Reynolds, 2013); austenitic laser-welded angles (Filipović, Dobrić, Buđevac, et al., 2021); austenitic cold-formed angles (Dobrić et al., 2020; Zhang, Tan, and Zhao, 2019); and austenitic hot-rolled angles (de Menezes et al., 2019; Sarquis et al., 2020; Behzadi-Sofiani, Gardner, and Wadee, 2021; Filipović, Dobrić, Baddoo, et al., 2021). Comparisons to existing design provisions including Design Guide 27 have found that the existing design provisions were conservative, especially for short columns exhibiting flexural-torsional buckling (Zhang, Tan, and Zhao, 2019; Sarquis et al., 2020; Dobrić et al., 2020; Behzadi-Sofiani, Gardner, and Wadee, 2021; Filipović, Dobrić, Baddoo, et al., 2021; Filipović, Dobrić, Buđevac, et al., 2021).

Despite the increase in data for equal-leg angles, only minimal existing research on unequal-leg angles subjected to uniform compression, and none for stainless steel members, was located. Early work by Liu and Chantel (2011) considered 26 carbon steel unequal-leg angles subjected to compression with varying amounts of eccentricity. All five concentrically loaded angles failed primarily in flexural buckling at less than 40% of the yield stress. Dinis et al. (2015) evaluated four carbon steel unequal-leg angles to investigate the elastic flexural-torsional response in asymmetric sections. Experimental results and subsequent modeling were found to be in agreement with the standard theoretical elastic buckling capacity used in the AISC Specifications. Ojalvo (2011) summarized the results of three fixed end aluminum unequal-leg angles tests (Liao, 1982; Wu, 1982). As noted by Dinis et al. (2015), the inelastic response of the fixed ended columns captured additional post-critical strength excluded in the standard elastic buckling assumptions. Recently, Zhang, Wang, et al. (2020) and Zhang, Bu, et al. (2021) tested 22 pinned end aluminum unequal-leg angle columns. Experimental results consistently exhibited flexural-torsional buckling; however, the response was dominated by torsional behavior at short lengths with a gradual transition to significant flexural behavior at long lengths.

This paper summarizes the progress on an ongoing study of stainless steel unequal-leg angles subjected to concentric compression. A companion experimental study on hot-rolled stainless-steel unequal-leg angles was previously reported by the authors (Laracuate, Sippel, and Blum, 2022). The goal is to expand the limited research on the behavior of this asymmetric shape and to inform design requirements for stainless steel unequal-leg angles in compression.

2. Material Properties

The cross-section tested was a laser-fused 76.2 x 50.8 x 6.35 mm (3" x 2" x 1/4") angle in Grade 304/304L austenitic stainless steel. Table 1 presents the chemical composition of the tested material, as reported in the manufacturer's mill certificate.

Table 1: Chemical composition of tested stainless steel angles

	Chemical Composition (Weight %)											
	Al	C	Cr	Cu	Mn	Mo	N	Ni	P	S	Si	Ti
Web	-	0.018	18.088	0.465	1.843	0.425	0.082	8.097	0.031	0.001	0.188	-
Flange	-	0.018	18.088	0.465	1.843	0.425	0.082	8.097	0.031	0.001	0.188	-

2.1 Tensile Coupon Test

To obtain the material properties of the studied laser-fused stainless steel angle section, a series of tensile coupon tests were performed. All coupons were cut from two 254 mm segments from A3 and A4. From each 254 mm segment 3 coupons were cut, one coupon from the middle portion of the 50.8 mm leg and two coupons from the 76.2 mm leg in the longitudinal direction (see Fig. 1). The coupons were all given a unique name which identifies the angle it was cut from and the number. For example, with coupon LC254-A3-1, 'LC254-A3' represents a coupon cut from the 254 mm piece A3, and '1' represents this is the first coupon cut from the 254 mm piece. The coupon dimensions were chosen to meet the requirements specified in the ASTM E8/E8M-16a (ASTM, 2016). A total of 6 tensile tests were conducted using (i) an MTS Criterion 43 with a 50-kN capacity and (ii) an MTS 810 Servo-Hydraulic frame with a 445-kN capacity. Two different machines were used because the MTS 810 Servo-Hydraulic frame did not have the capacity for three outputs and the MTS Criterion 43, which had three outputs, did not have the capacity to run the test up to ultimate and fracture. Thus a combination was used to ensure adequate data was captured in the elastic range and at ultimate. For the coupons tested on the MTS Criterion 43, the instrumentation used included: (i) two linear electrical resistance strain gauges attached at mid-height to the center of the front and back faces of the coupons to determine the average strains in the longitudinal direction, and (ii) an extensometer with a 50.8 mm gauge length to obtain the average strain over the gauge length. For the coupons tested on the MTS 810 Servo-Hydraulic frame, only the 50.8 mm gauge length extensometer was used to record the strains. The engineering stress-strain curves obtained from the tensile coupon tests are shown in Fig.1. These curves represent static material properties and were obtained following the procedure proposed by Huang and Young (2014). Curves plotted with a dashed line represent the tests conducted using the MTS Criterion 43 with a 50-kN capacity. Fig. 1 contains a legend that depicts the locations in the cross-section where each tensile coupon was cut. Table 2 summarizes the results obtained from these tests, where E is the Young's modulus, f_y and $f_{1.0}$ are the 0.2% and 1.0% proof stresses, respectively, and n and $n_{0.2,1.0}$ are the Ramberg–Osgood strain hardening exponents, with $n_{0.2,1.0}$ corresponding to a model proposed by Arrayago et al. (2015).

2.2 Residual Stress Measurement

The distribution of residual stresses for the hot-rolled stainless steel unequal-leg angles was measured through the sectioning method. The steps are as follows:

1. A 610 mm long angle was cut from stock and then a 305 mm long test piece was marked on

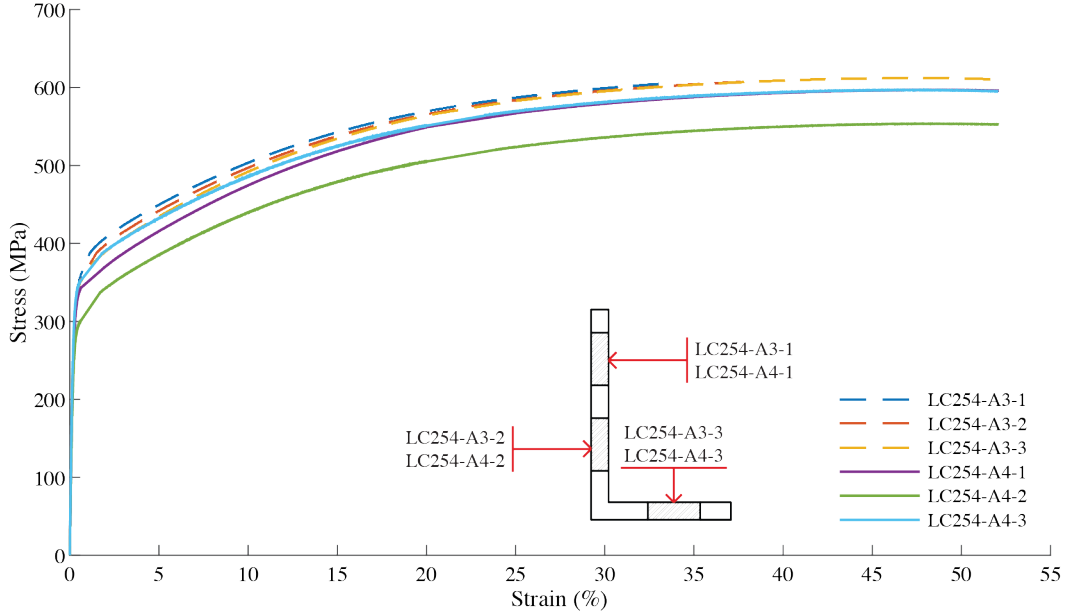


Figure 1: Measured stress-strain curves from coupon tests. The dashed lines indicate that the specimen was tested in equipment with reduced capacity.

Table 2: Measured material properties

Specimen	E (MPa)	f_y (MPa)	$f_{1.0}$ (MPa)	n	$n_{0.2,1.0}$
LC10-A3-1	183792	331.9	390.4	6.22	1.80
LC10-A3-2	179589	329.1	376.6	5.28	2.27
LC10-A3-3	172394	329.0	372.1	6.20	2.31
LC10-A4-1	158197	325.0	355.0	6.88	2.96
LC10-A4-2	152256	286.6	320.6	7.63	1.73
LC10-A4-3	181889	337.4	369.5	7.31	1.89
Average	171353	323.2	364.0	6.58	2.16
Nominal	193000	205.0	-	7.00	-

the center of the 610 mm piece. This was done because a distance of 2.0 times the lateral dimension is recommended to reduce end effects on the tests piece (Tebedge, Alpsten, and Tall, 1973). The 305 mm test piece was then marked into 20 strips with a strip width of 6.35 mm.

2. For each cross-sectional strip, two 1.59 mm diameter gauge holes were drilled 254 mm apart (on center) in the longitudinal direction. After the specimen was left at room temperature for two hours, the distance between the gauge holes were measured using the Humboldt multi-length strain gauge with a precision of 0.0025 mm to obtain the initial gauge length measurements.
3. The 305 mm long test piece was cut from the 610 mm long piece using a horizontal bandsaw with cutting coolant flowing constantly across the cut.
4. The test piece was cut into twenty 305 x 6.35 mm strips using a waterjet. The strips, as shown in Fig. 2, were again left for two hours at room temperature before the new gauge length measurements of each strip were recorded.



Figure 2: Angle cut into strips through the sectioning method

The residual stresses were calculated using Eq. 1 where E_o is the initial modulus of elasticity, L_f is the final length of the strip, and L_i is the initial length of the strip.

$$\sigma_r = -E_o \frac{(L_f - L_i)}{L_i} \quad (1)$$

Fig. 3 shows the residual stress distribution obtained for the laser-fused stainless steel unequal-leg angle for both inside and outside faces. The vertical left axis of the plot represents the stress in MPa and the vertical right axis represents the stress normalized by the measured 0.2% proof stress from the tensile coupon tests. On both axes, positive values represent residual tensile stresses and negative values represent residual compressive stresses. The horizontal axis represents the distance in mm from the heel of the angle to the ends of each leg. Nine strips closer to the heel on the inside face could not have an initial measurement prior to cutting the piece into strips due to the size of the Humboldt multi-length strain gauge dial; this created a gap in the data for the inside face distribution. For the outer face, the maximum compressive residual stress was determined to be approximately 88 MPa ($0.3F_y$) and the maximum tensile residual stress was approximately 101 MPa ($0.35F_y$). The observed magnitude and distribution of residual stress measurements for the outer face are similar in range to what previous researchers measured for laser-fused stainless steel equal-leg angles (Filipović, Dobrić, Buđevac, et al., 2021).

3. Column Buckling Test

The investigation focused on testing unequal-leg stainless steel angles under axial compression. All specimens were tested through failure to approximately 80% post ultimate load. The initial geometric imperfections of each specimen were measured but are not included in this paper; results will be presented in a future publication. All specimens were cut from six separate 6 meter-long angles, which were labeled A1 to A6. Each specimen was given a unique name which identifies the nominal length, the angle it was cut from, and the number. For example, with specimen L914-A1-2, ‘L914’ represents a specimen with a 914 mm (36”) length, ‘A1’ represents the specimen was cut from angle A1, and ‘2’ represents this is the second 914 mm specimen cut from angle A1. The cross-section tested was a laser-fused 76.2 x 50.8 x 6.35 mm (3” x 2” x 1/4”) angle. Table 3 shows the geometric properties of the specimens used in this study, where L is the length of the specimen, b and h are the width and height of the section, respectively, t_h is the thickness of the 76.2 mm leg, and t_b is the thickness of the 50.8 mm leg as shown in Fig. 4.

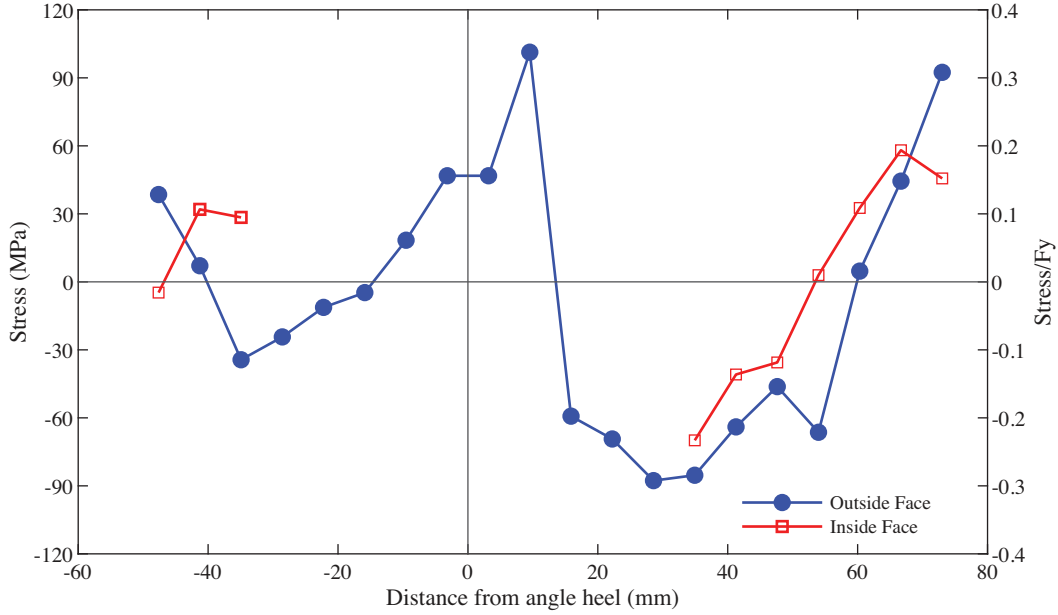


Figure 3: Residual stress distribution

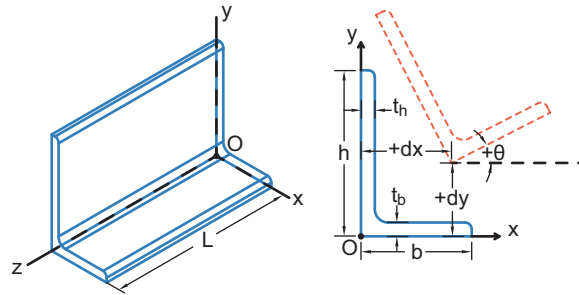


Figure 4: Unequal-leg angle conventions for dimensions, axes, and displacements

3.1 Test Setup

A series of compression tests were completed on 18 laser-fused Grade 304/304L austenitic stainless steel unequal-leg 76.2 x 50.8 x 6.35 mm (3" x 2" x 1/4") angles, with lengths ranging from 254 mm (10") to 3759 mm (148"), to measure their buckling response and load-carrying capacity. All tests were conducted in a Southwark Emery Testing Machine with a capacity of 4,448 kN (1 million pounds) in tension and compression. A 445 kN (100 kips) load cell attached to the cross head of the testing machine was used to measure the applied load during testing. All tests were performed in a displacement control mode with a constant axial displacement rate of 0.0381 mm/min (0.0015 in/min). This rate allowed the specimens to be tested under quasi-static conditions. All tests were stopped when the load reached 80% post ultimate load. To quantify the average strains at mid-height, two linear electrical resistance strain gauges were attached to the center of the front and back faces of both legs, as shown in Fig. 5. To record the displacements and twists of each specimen, an optical tracking system with an overall accuracy of 0.1 mm (0.004 in) was used. The translations of four markers, two per leg on the outside face of the angle as shown in Fig. 5, were tracked at each elevation of interest. This information was converted to the lateral position and twist of the cross-section by calculating the best-fit angle orientation among all sensors as illustrated in Fig. 6, which incorporated two-dimensional data from each sensor. For the majority of the

Table 3: Measured geometric properties of test specimens

Specimen	L (mm)	b (mm)	h (mm)	t_b (mm)	t_h (mm)	Area (mm ²)
L254-A1-1	254	50.32	76.25	6.17	6.21	745.34
L254-A2-1	254	50.48	76.27	6.20	6.20	747.81
L254-A3-1	256	50.30	76.26	6.21	6.21	747.41
L508-A2-1	508	49.94	76.29	6.19	6.25	747.38
L508-A2-2	508	50.32	76.28	6.21	6.22	748.27
L508-A4-1	508	50.19	76.27	6.20	6.22	746.79
L914-A1-1	916	50.12	76.26	6.15	6.21	743.73
L914-A1-2	914	50.13	76.23	6.16	6.21	743.75
L914-A2-1	914	49.97	76.31	6.19	6.20	744.45
L1829-A3-1	1829	50.13	76.22	6.22	6.20	745.80
L1829-A5-1	1830	50.11	76.22	6.19	6.20	744.63
L1829-A6-1	1829	50.04	76.25	6.14	6.18	740.38
L2540-A4-1	2540	50.18	76.29	6.21	6.20	746.45
L2540-A4-2	2542	50.25	76.25	6.21	6.20	746.63
L2540-A5-1	2540	50.22	76.26	6.19	6.20	745.02
L3759-A1-1	3759	50.14	76.28	6.16	6.21	744.51
L3759-A2-1	3759	50.03	76.32	6.20	6.24	748.04
L3759-A3-1	3761	50.15	76.27	6.21	6.22	747.05

tests performed, this information was obtained near the ends, at quarter points, and at mid-span. For the smaller length specimens, a reduced number of markers were placed along the member length; for the longer lengths, an increased number of markers were used.

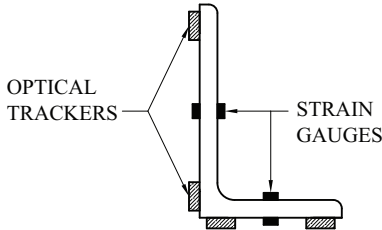


Figure 5: Position of the optical trackers and strain gauges

All tests were performed under fixed boundary conditions using a setup similar to the setup of Zhang et al. (2019), where the ends of the angle were restrained by fabricated steel plates (see Fig. 7). While the bottom plate was situated directly on the floor, the top plate was bolted to a thicker plate which was connected to the load cell, and this was gripped to the cross head of the testing machine. Both top and bottom plates were aligned with the centroid of the unequal-leg angle cross-section to ensure pure axial compression. The column buckling test setup used for all experiments is presented in Fig. 8.

3.2 Results

The failure loads obtained from the axial compression tests performed on all eighteen specimens are summarized in Table 4. From the results obtained it was observed that the majority of the specimens of each length failed at similar maximum loads with a coefficient of variation ranging from 1-9%. A graphical representation of the results obtained from the compression tests are shown in Figs. 9 - 14. These plots quantify how much each specimen displaced laterally, in the x- and y-

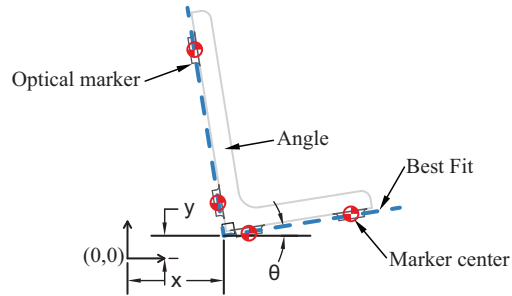


Figure 6: Fitting angle orientation and position to marker translations



Figure 7: End plates used to achieve fixed boundary conditions

directions, and how much they twisted at mid-height. The origin of the coordinate system is located at the heel of the angle, with the x-axis parallel to the 50.8 mm leg and the y-axis parallel to the 76.2 mm leg, as shown in Fig. 4. To compare the nominally identical specimens, corresponding results were plotted on the same figure. All plots show (1) that there is good agreement in the maximum displacements and rotations observed between nominally identical specimens, and (2) that all specimens of the same length buckled in the same direction. The plots for the 914 mm, 1829 mm, 2540 mm, and 3759 mm specimens show the slight variation that exists in the maximum loads between nominally identical specimens. The plots for the 2540 mm and 3759 mm specimens show that after peak-load was reached, a sudden loss in the strength capacity of the members occurred. The plots for some 508 mm, 914 mm, 1829 mm, 2540 mm, and 3759 mm specimens show a black dashed line from the origin to approximately 9 kN; it represents an interpolation of the data in this region. Before starting each test, all specimens were preloaded to approximately 9 kN to prevent misalignment of the top and bottom plates during the bolt tightening process necessary to restrain the angle. For some of the tests, the preload decreased with time before data recording began and interpolation was not necessary. For the specimens where preload did not decrease, data collection started approximately at 9 kN.

Fig. 15 shows the position of a cross-section at mid-height at the start of the test, peak load, and 80% post-peak load of a single specimen in each length. At the shorter lengths, 254 mm and 508 mm specimens, it was observed that the behavior mainly consisted of rotations with no significant lateral displacements (see Figs. 15a & 15b). At the intermediate lengths, 914 mm and 1829 mm

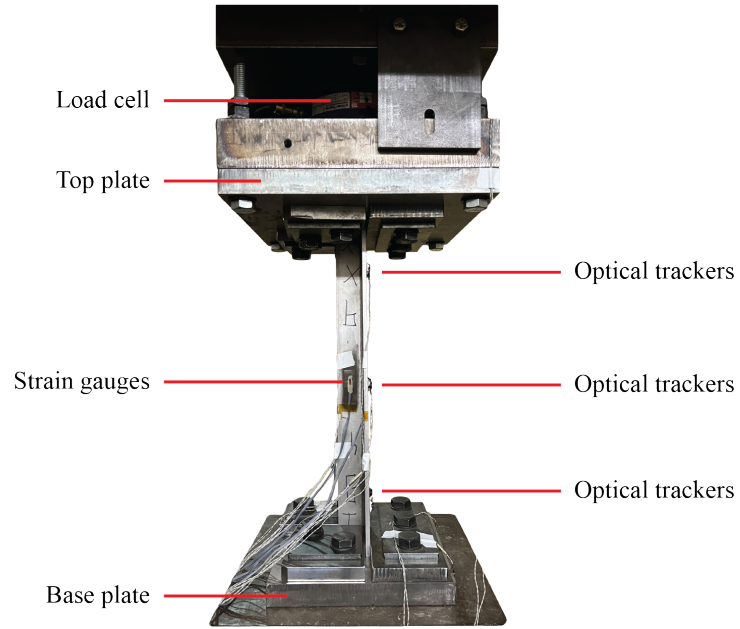


Figure 8: Typical test setup

specimens, rotations were reduced as compared to the shorter lengths and flexural mode began to participate in the overall failure mode (see Figs. 15c & 15d). At the longer lengths, 2540 mm and 3759 mm specimens, the flexural mode had the biggest participation in the overall behavior of the section due to some significant lateral displacements and small rotations when compared to the shorter specimens (see Figs. 15e & 15f). In general, the results obtained from the experimental investigation show that flexural-torsional buckling was the dominant failure mode at short lengths and flexural buckling at long lengths, with a gradual transition occurring in the middle lengths. Fig. 16 illustrates some photographs of the buckled specimens taken during the compression tests performed on the various laser-fused stainless steel angles.

Table 4: Experimental failure loads

Specimen	Load (kN)	Mean	Standard Deviation	COV (%)
L254-A1-1	265.8			
L254-A2-1	258.8	261.7	3.7	1.4
L254-A3-1	260.4			
L508-A2-1	227.9			
L508-A2-2	231.2	231.0	3.0	1.3
L508-A4-1	233.9			
L914-A1-1	209.0			
L914-A1-2	191.1	197.4	10.0	5.1
L914-A2-1	192.2			
L1829-A3-1	109.0			
L1829-A5-1	127.8	115.7	10.5	9.1
L1829-A6-1	110.4			
L2540-A4-1	74.9			
L2540-A4-2	72.7	76.1	4.2	5.5
L2540-A5-1	80.8			
L3759-A1-1	39.3			
L3759-A2-1	36.7	36.8	2.5	6.7
L3759-A3-1	34.3			

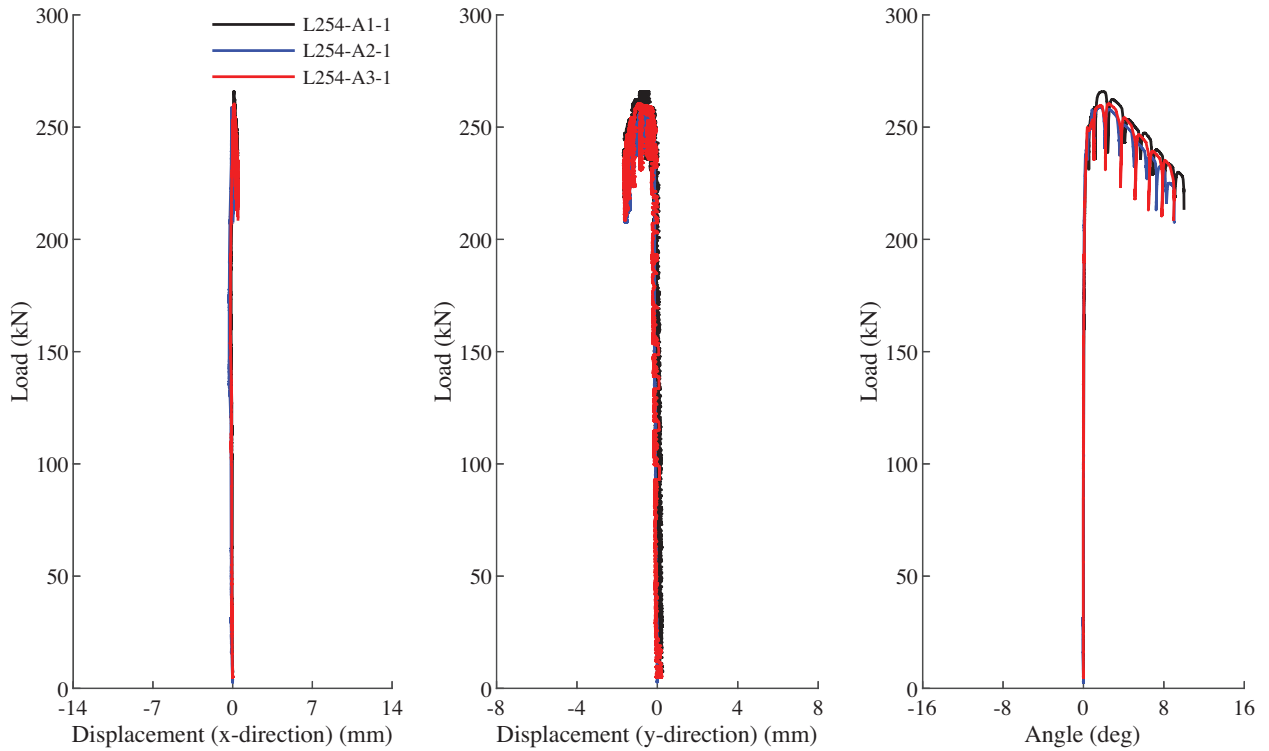


Figure 9: Displacement and rotations obtained for all 254 mm angles

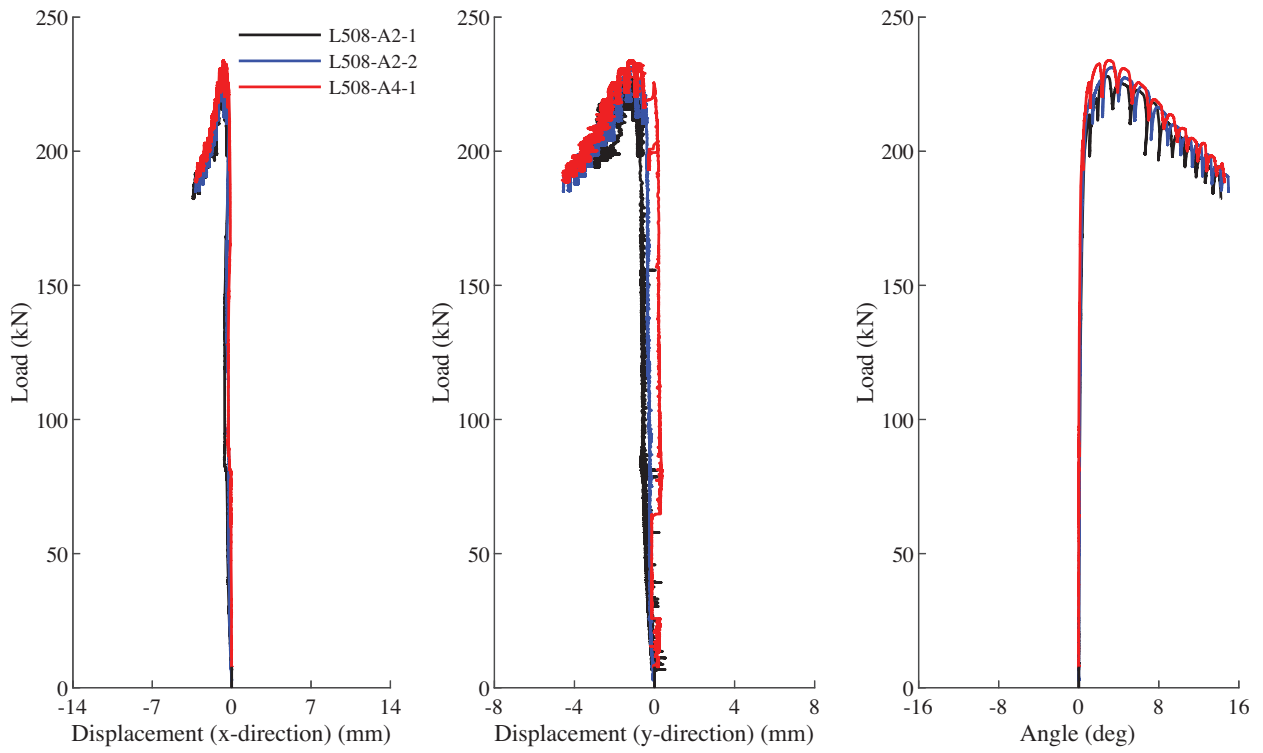


Figure 10: Displacement and rotations obtained for all 508 mm angles

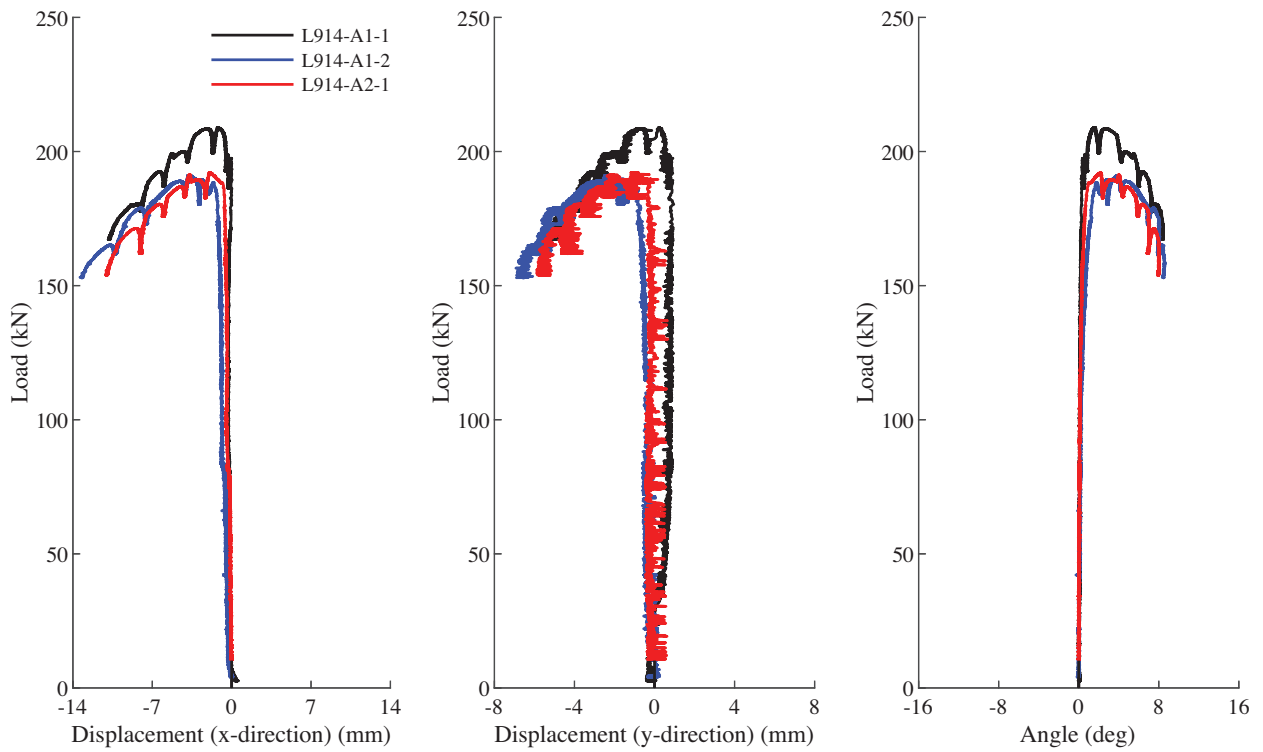


Figure 11: Displacement and rotations obtained for all 914 mm angles

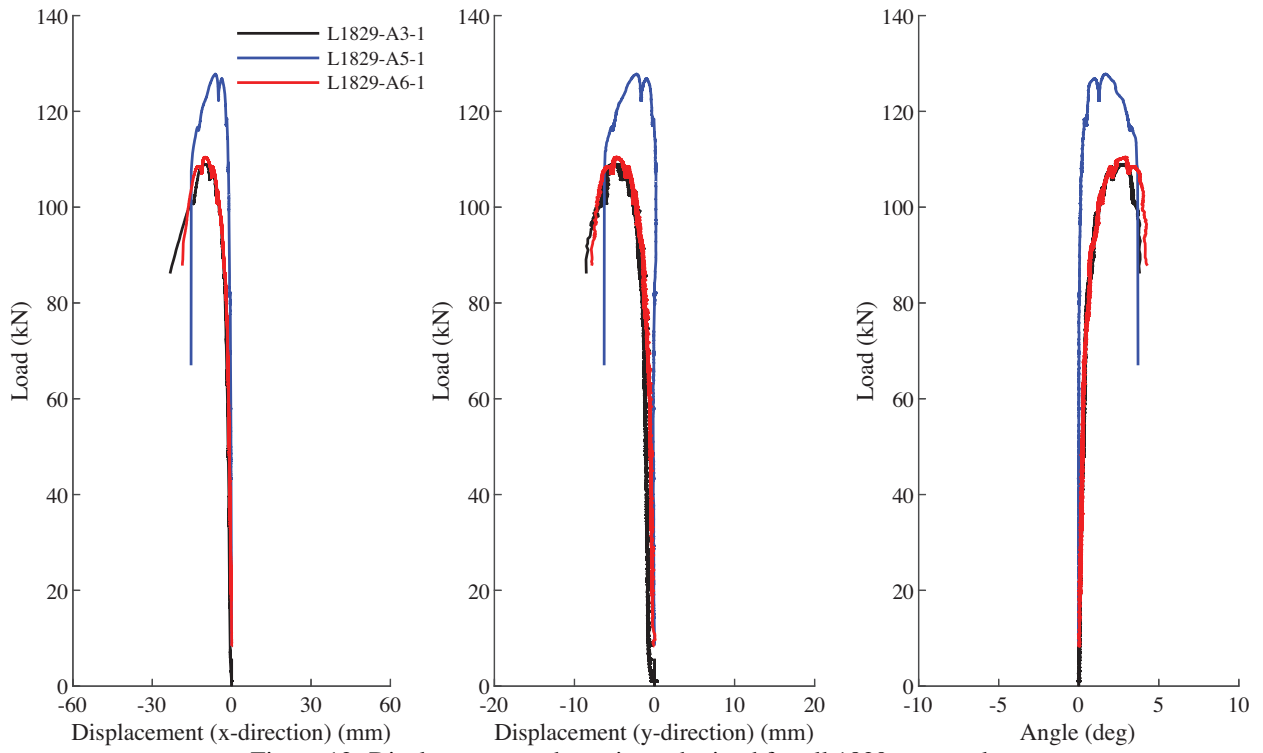


Figure 12: Displacement and rotations obtained for all 1829 mm angles

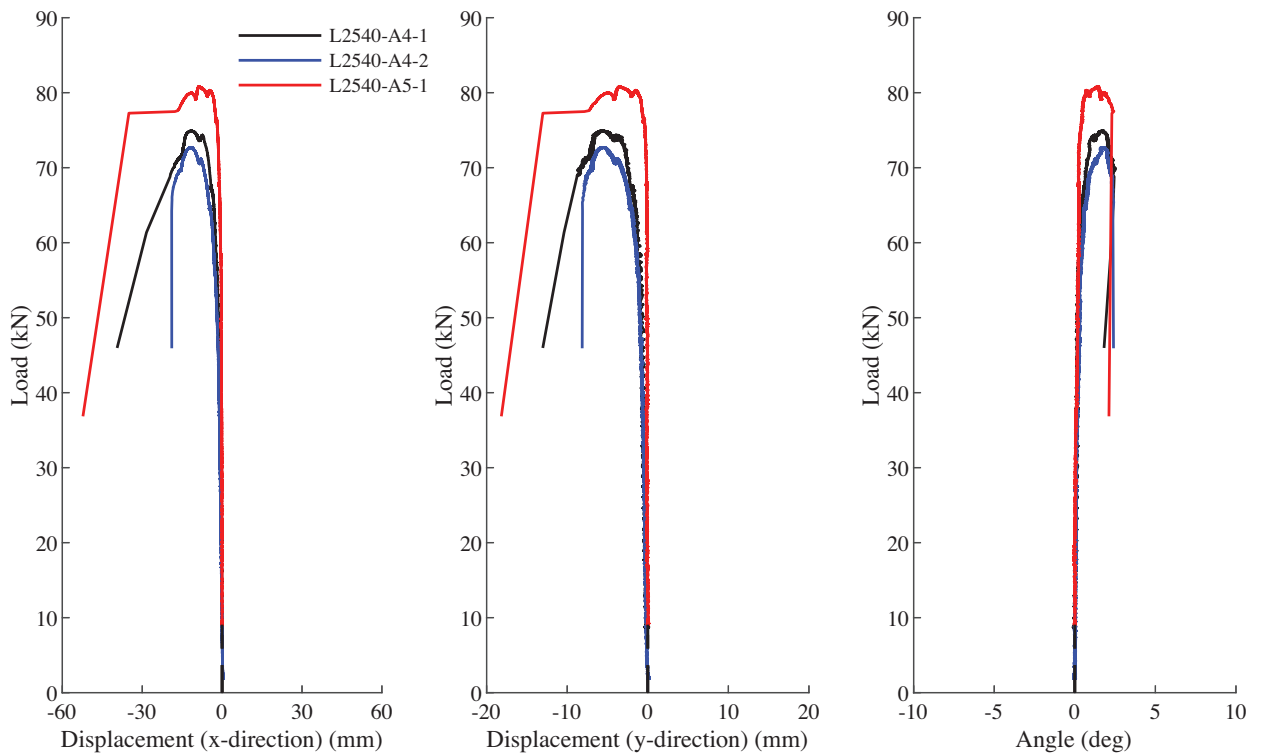


Figure 13: Displacement and rotations obtained for all 2540 mm angles

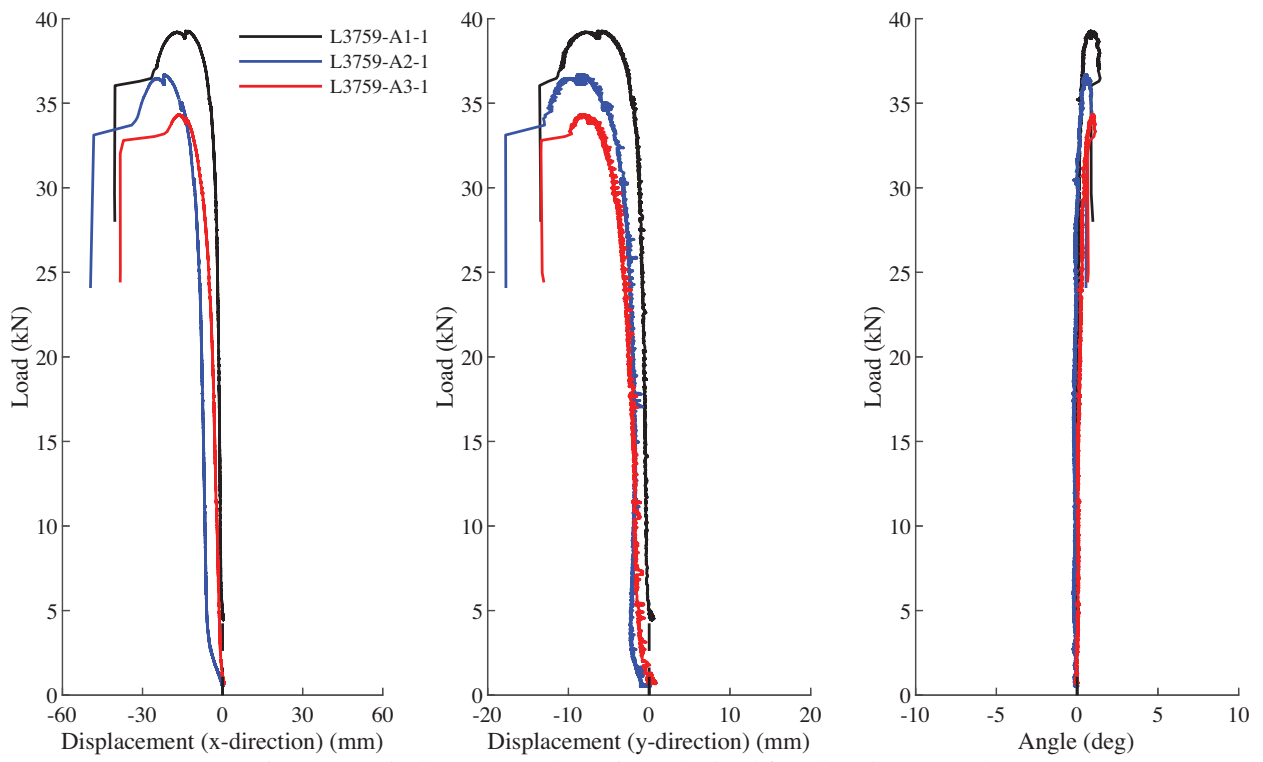


Figure 14: Displacement and rotations obtained for all 3759 mm angles

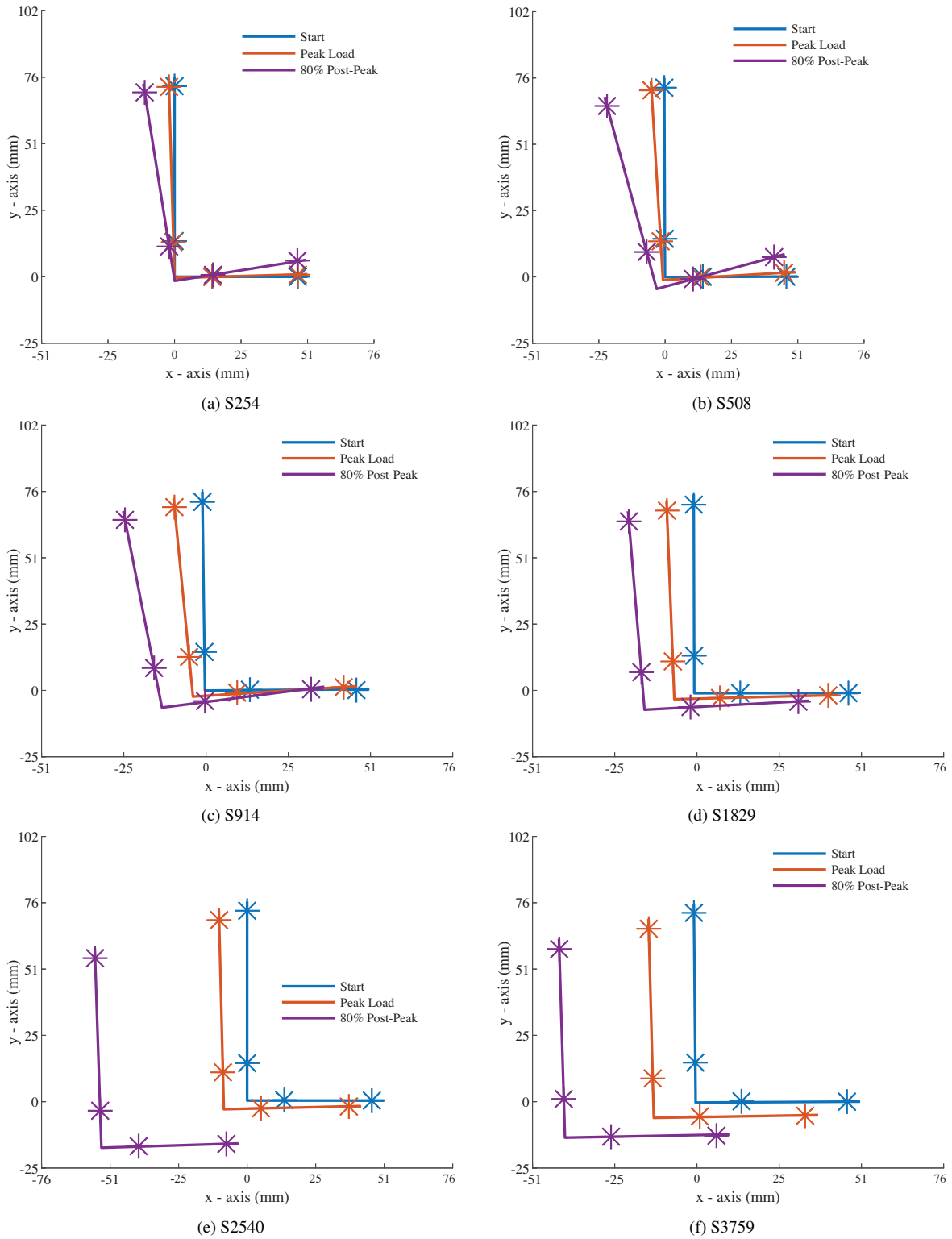


Figure 15: Cross-section mid-height position at start, peak load, and 80% post-peak of various specimens



a) L254



b) L508



c) L914



d) L1829



e) L2540



f) L3759

Figure 16: Photographs of buckled specimens

4. Conclusions

This paper presents the results of an experimental investigation performed on a series of stainless steel unequal-leg angles subjected to concentric compression. A total of 18 laser-fused 76.2 x 50.8 x 6.35 mm (3" x 2" x ¼") stainless steel angles of six different lengths ranging from 254 mm (10") to 3759 mm (148") were tested under axial compression through failure to 80% post-ultimate. During the experiments, displacements and twists were recorded along the full length of the member at quarter point intervals for all specimens. The data was analyzed to obtain the full behavior of each specimen and compare the failure modes across all lengths. Results show that all tested specimens failed in three different modes: (i) torsional mode, (ii) flexural mode, and (iii) flexural-torsional mode. It was found that the dominant failure mode was torsional buckling at very short lengths, flexural buckling at long lengths, and combined flexural-torsional buckling at intermediate lengths. As part of the experimental investigation, the material properties and the cross-section residual stresses of the tested stainless steel angles were measured. Through tensile coupon tests, it was observed that the measured material properties are approximately 58% higher than nominal values. The experimental data collected from this investigation will expand the limited research on the stability behavior of unequal-leg stainless-steel angles in compression.

Acknowledgements

The authors would like to thank Stainless Structural for material donations and the American Institute of Steel Construction for their financial assistance of the experimental component of the project. Support for the first author was provided by the Graduate Engineering Research Scholars Fellowship. Lastly, the authors would like to thank undergraduate researcher Gabriel Lepak for his assistance in completing the imperfection scanning and compression testing and Jacob Zeuske for his technical assistance with testing.

References

- AISC (2016). *Specification for Structural Steel Buildings ANSI/AISC 360-16*. Chicago, IL: American Institute of Steel Construction, p. 676.
- AISC (2021). *Specification for Structural Stainless Steel Buildings ANSI/AISC 370-21*. Chicago, IL: American Institute of Steel Construction, p. 376.
- Arrayago, I., E. Real, and L. Gardner (2015). "Description of stress-strain curves for stainless steel alloys". In: *Materials & Design* 87, pp. 540–552. DOI: <https://doi.org/10.1016/j.matdes.2015.08.001>.
- ASTM (2016). *Standard Test Methods for Tension Testing of Metallic Materials*. ASTM E8/EM8-16a. West Conshohocken, PA: American Society for Testing and Materials.
- Baddoo, Nancy R. (2013). *Structural Stainless Steel*. Design Guide 27. Chicago, IL: American Institute of Steel Construction, p. 150.
- Behzadi-Sofiani, Behnam, Leroy Gardner, and M. Ahmer Wadee (2021). "Stability and design of fixed-ended stainless steel equal-leg angle section compression members". In: *Engineering Structures* 249, p. 113281. DOI: [10.1016/j.engstruct.2021.113281](https://doi.org/10.1016/j.engstruct.2021.113281).
- de Menezes, Arthur A., Pedro C. G. da S. Vellasco, Luciano R. O. de Lima, and André T. da Silva (2019). "Experimental and numerical investigation of austenitic stainless steel hot-rolled angles under compression". In: *Journal of Constructional Steel Research* 152, pp. 42–56. DOI: [10.1016/j.jcsr.2018.05.033](https://doi.org/10.1016/j.jcsr.2018.05.033).

- Dinis, Pedro B., Dinar Camotim, Kostas Belivanis, Colter Roskos, and Todd A. Helwig (2015). “On the buckling, post-buckling and strength behavior of thin-walled unequal-leg angle columns”. In: *Proceedings of the 2015 SSRC Annual Stability Conference*. Nashville, TN: SSRC, pp. 1–15.
- Dobrić, Jelena, Aljoša Filipović, Zlatko Marković, and Nancy R. Baddoo (2020). “Structural response to axial testing of cold-formed stainless steel angle columns”. In: *Thin-Walled Structures* 156, p. 106986. DOI: 10.1016/j.tws.2020.106986.
- Filipović, Aljoša, Jelena Dobrić, Nancy R. Baddoo, and Primož Može (2021). “Experimental response of hot-rolled stainless steel angle columns”. In: *Thin-Walled Structures* 163, p. 107659. DOI: 10.1016/j.tws.2021.107659.
- Filipović, Aljoša, Jelena Dobrić, Dragan Buđevac, Nenad Fric, and Nancy R. Baddoo (2021). “Experimental study of laser-welded stainless steel angle columns”. In: *Thin-Walled Structures* 164. DOI: 10.1016/j.tws.2021.107777.
- Galambos, Theodore V. (1991). “Design of axially loaded compressed angles”. In: *Proceedings of the 1991 SSRC Annual Stability Conference: "Inelastic Behavior and Design of Frames"*. Chicago, IL: SSRC, pp. 353–367.
- Houska, Catherine (2014). *Designing Stainless Steel Part 1*. Conference Presentation. NASSC: The Steel Conference. Toronto, Canada.
- Huang, Yuner and Ben Young (2014). “The art of coupon tests”. In: *Journal of Constructional Steel Research* 96, pp. 159–175. DOI: <https://doi.org/10.1016/j.jcsr.2014.01.010>.
- Kuwamura, Hitoshi (2003). “Local buckling of thin walled stainless steel members”. In: *Steel Structures* 3, pp. 191–201.
- Laracuenta, Max E., Edward J. Sippel, and Hannah B. Blum (2022). “Stability considerations of unequal-leg angle stainless steel columns”. In: *Proceedings of the 2022 SSRC Annual Stability Conference*. Denver, CO: SSRC, pp. 1–20.
- Liao, KY (1982). “Compression tests of unequal-leg angles”. MA thesis. Ohio State University.
- Liu, Yi and Sabine Chantel (2011). “Experimental study of steel single unequal-leg angles under eccentric compression”. In: *Journal of Constructional Steel Research* 67.6, pp. 919–928. DOI: 10.1016/j.jcsr.2011.02.005.
- Ojalvo, Morris (2011). “Opposing Theories and the Buckling Strength of Unequal-Leg Angle Columns”. In: *Journal of Structural Engineering* 137.10, pp. 1104–1106. DOI: 10.1061/(ASCE)ST.1943-541X.0000389.
- Reynolds, Nicholas A. (2013). “Behavior and Design of Concentrically Loaded Duplex Stainless Steel Single Equal-Leg Angle Struts”. PhD Dissertation. Georgia Institute of Technology, p. 253.
- Sarquis, Fernando R., Luciano R. O. de Lima, Pedro C. G. da S. Vellasco, and Monique C. Rodrigues (2020). “Experimental and numerical investigation of hot-rolled stainless steel equal leg angles under compression”. In: *Thin-Walled Structures* 151, p. 106742. DOI: 10.1016/j.tws.2020.106742.
- Sun, Yao, Zhanke Liu, Yating Liang, and Ou Zhao (2019). “Experimental and numerical investigations of hot-rolled austenitic stainless steel equal-leg angle sections”. In: *Thin-Walled Structures* 144, p. 106225. DOI: 10.1016/j.tws.2019.106225.
- Tebedge, N, G Alpsten, and LJEM Tall (1973). “Residual-stress measurement by the sectioning method”. In: *Experimental Mechanics* 13.2, pp. 88–96.

- Wu, Fu-hsiang (1982). “Experimental Determination of Buckling Loads for Unequal Leg Angles with Concentric Loads”. MA thesis. Ohio State University.
- Zhang, Lulu, Kang Hai Tan, and Ou Zhao (2019). “Experimental and numerical studies of fixed-ended cold-formed stainless steel equal-leg angle section columns”. In: *Engineering Structures* 184, pp. 134–144. DOI: 10.1016/j.engstruct.2019.01.083.
- Zhang, Ying, Yidu Bu, Yuanqing Wang, Zhongxing Wang, and Yuanwen Ouyang (2021). “Study of flexural–torsional buckling behaviour of 6061-T6 aluminium alloy unequal-leg angle columns”. In: *Thin-Walled Structures* 164, p. 107821. DOI: 10.1016/j.tws.2021.107821.
- Zhang, Ying, Yuanqing Wang, Zhongxing Wang, Yidu Bu, Shenggang Fan, and Baofeng Zheng (2020). “Experimental investigation and numerical analysis of pin-ended extruded aluminium alloy unequal angle columns”. In: *Engineering Structures* 215, p. 110694. DOI: 10.1016/j.engstruct.2020.110694.